High Homogeneity of Magnesium Doped LiNbO₃ Crystals Grown by Bridgman Method

Xiaodong Yan, Tian Tian *, Menghui Wang, Hui Shen, Ding Zhou, Yan Zhang and Jiayue Xu *

Institute of Crystal Growth, School of Materials Science and Engineering, Shanghai Institute of Technology, Shanghai 201418, China; 176081108@mail.sit.edu.cn (X.Y.); wmh_fzs@163.com (M.W.); hshen@sit.edu.cn (H.S.); dzhou@sit.edu.cn (D.Z.); yanzhang@sit.edu.cn (Y.Z.)

* Correspondence: tiant@sit.edu.cn (T.T.); xujiayue@sit.edu.cn (J.X.); Tel.: +86-021-608-731-17 (T.T.); +86-021-608-734-89 (J.X.); Fax: +86-021-608-731-17 (T.T.); +86-021-608-734-89 (J.X.)

check for updates

Abstract: A series of LiNbO₃ crystals doped with various MgO concentrations (0, 3%, and 5 mol%) was simultaneously grown in one furnace by the modified vertical Bridgman method. The wet chemistry method was used to prepare the polycrystalline powders, and the growth conditions were optimized. The full width at half maximum of high-resolution X-ray rocking curves for (001) reflection of 5 mol% Mg doped lithium niobate (LN) crystal was about 8″, which meant it possessed high crystalline quality. The OH⁻ absorption spectra shifted to 3534.7 cm⁻¹, and the UV absorption edge violet shift indicated that 5 mol% MgO successfully doped in LN and exceeded the threshold. The extraordinary refractive index gradient of 5 mol% Mg doped LN crystal was as small as 2.5×10^{-5}/cm, which exhibited high optical homogeneity.

Keywords: lithium niobate; doping magnesium; Bridgman method; high homogeneity

1. Introduction

Lithium niobate (LiNbO₃, or LN) crystal is one of the most prominent materials for applications in many practical fields, such as optical modulators [1], holographic storage [2], waveguides [3,4], resonators [5], integrated optics devices and three-dimensional (3D) displays, resulting from its superior and diverse physical performance [6,7]. Since the first successful growth by Czochralski method in 1965 [8], crystal growth, photorefractive properties, and theoretical simulations have been studied in depth, and substantial research progress has been reported for LN crystals [9–14]; for example, Ø6″ pure LN crystals with high homogeneity has been reported recently [15].

Normally, LN is a non-stoichiometric compound, and the (Li)/(Nb) ratio of congruent composition is 48.38/51.62 [16,17]. According to the broadly accepted Li-vacancy model, the congruent composition induces a large concentration of intrinsic defects that exist in LN, which mainly are Li vacancies (V_{Li}^-) and anti-site Nb^{5+} (Nb_{Li}^{4+}). Small polarons (an electron trapped at Nb_{Li}^{4+}) together with bipolarons (a pair of electrons trapped at adjacent Nb_{Li}^{4+} and Nb_{Nb}^{5+}) play the role of laser-induced optical damage (also named photorefraction) centers in LN [10]. The serious disadvantage of laser-induced optical damage in LN limits its usability in nonlinear optical applications [18]. Doping optical damage resistant additives into LN crystal is an effective approach to suppress the optical damage; especially, Zhong et al. first reported that the laser-induced optical damage could be suppressed by doping MgO with high concentration, exceeding its threshold (about 5 mol%) [19]. The mechanism is when the concentration of MgO exceeded its threshold, Mg^{2+} repelled anti-site Nb^{5+} to the site of normal-Nb. Thereby, the formation of small polarons and bipolarons, which serve as an optical damage center, are suppressed remarkably [20]. This discovery impelled magnesium doped LN (LN:Mg) crystals to play a significant role in nonlinear optics and have achieved industrial growth. Consequently, a summarized
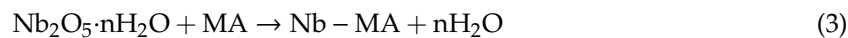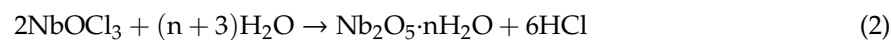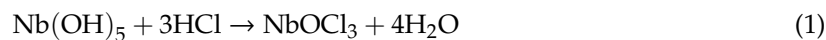
result of researches on optical grade heavily Mg-doped LN crystals has revealed that most of them have been grown by the Czochralski method with the diameter of Ø1"–2", and the homogeneity has not been satisfactory [21–25]. Furthermore, only one crystal can be grown in one furnace each time by the Czochralski method, which indicates low growth efficiency.

Bridgman method is one of the main methods for industry crystal growth, such as optical crystals [26], piezoelectric crystals [27,28], ferroelectric crystals [29], and semiconductor crystals [30,31], for its many advantages, especially multiple crystals can be grown in one furnace at the same time, which means high production efficiency. However, there are few reports about the preparation of lithium niobate by the Bridgman method [32,33], especially growing large optical grade heavily Mg-doped LN crystals with high homogeneity is still difficult. Since the lithium niobate crystal belongs to the trigonal crystal system, the crystal is easy to crack. According to previous reports, the growth of crystals becomes more difficult as the concentration of magnesium is increased because the high concentration of MgO in the melt cause (Li)/(Nb) ratio extremely deviate from the congruent composition [34,35]. Besides, the segregation coefficient of MgO deviated from one could induce inhomogeneity along the growth direction [36]. So, the growth process of the Bridgman method for LN:Mg crystals should be optimized.

In this study, we used the Bridgman method to grow Ø2" LN crystals with different concentrations of magnesium ions. In order to obtain Ø2" heavily Mg-doped LN with high homogeneity, systematically optimized scheme, including polycrystalline powers preparation, thermal field design, and growth technologies of the Bridgman method, was demonstrated in this work. The homogeneity of LN: Mg crystals was also checked.

2. Materials and Methods

LN:Mg polycrystalline powders were synthesized by a wet chemistry method. $Nb(OH)_5$ (99.99%) was firstly weighted, and excess HCl (38%) was added into a container. Then, they were heated at 90 °C and stirred for 30 min. During this process, the mass of active $Nb_2O_5 \cdot nH_2O$ was precipitated. After being cooled, the observed white precipitate was $NbOCl_3$, which should be completely dissolved by adding deionized water. Malic acid ($C_4H_6O_4$, MA) as the ratio of (MA):(Nb) = 3:1 was added into the former solution and stirred. Then, the pH value of the suspension was adjusted to 8 by the addition of $NH_3 \cdot H_2O$ to get solution A. The chemical reactions happened in producing solution A were as follows:

$$Nb(OH)_5 + 3HCl \rightarrow NbOCl_3 + 4H_2O \tag{1}$$

$$2NbOCl_3 + (n+3)H_2O \rightarrow Nb_2O_5 \cdot nH_2O + 6HCl \tag{2}$$

$$Nb_2O_5 \cdot nH_2O + MA \rightarrow Nb - MA + nH_2O \tag{3}$$

According to the congruent composition of (Li)/(Nb) = 48.38/51.62 and the selected doping concentration of MgO (0, 3 mol%, 5 mol%), Li_2CO_3 (99.99%) and MgO (99.99%) were weighted and dissolved by dilute HCl. Until no more bubbles produced, the pH value was adjusted to 8 by the addition of $NH_3 \cdot H_2O$ to get solution B. Afterward, solutions A and B were mixed to be of high homogeneity by ultrasonic machine. The mixed solution was filtered and spray dried into powders. At last, the powders were sintered at 820 °C for 6 h to obtain LN:Mg polycrystalline powders.

Using the prepared LN:Mg polycrystalline powder, we firstly grew Ø1" LN:Mg crystals and served them as seed crystals continue to grow Ø2" LN crystals doped with different MgO concentration of 0, 3%, and 5 mol% by the Bridgman method with multi-crucible [31], which were labeled as LN, LN: Mg3, and LN: Mg5, respectively. The prepared LN: Mg polycrystalline powder was placed in three Pt crucibles with the same dimension of Ø50 mm × 100 mm. After putting them into three Al_2O_3 pipes with the dimension of Ø110 mm × 200 mm, they were simultaneously placed in a furnace. Some mullite fiber mixed with Al_2O_3 powders was used as the thermal insulation material to keep a stable thermal field. In order to be sufficiently melted, the LN: Mg polycrystalline powder was heated

by medium-frequency induction and held at 100 °C above the melting point for 2 h. LN, LN: Mg3, and LN: Mg5 crystals were grown in a sealed environment and along the c-axis. In the procedure of crystal growth, the falling rate was governed in the range of 0.5 mm/h to 1.0 mm/h. The vertical temperature gradient above the solid-melt interface was about 0.3 °C/mm, which was measured by using a thermocouple. In order to avoid the cracks occurring in large crystals, they were cooled down to room temperature at a low rate of 30 °C/h after the growth process. Finally, LN: Mg crystals with Ø2″ in diameter and 40 mm in length were grown along the c axis. It was necessary to anneal the as-grown crystals at 1230 °C for 30 h to escape thermoelastic stress and improve optical homogeneity. The single-domain structure would be formed by polarization with an electric current density of 7 mA/cm^2 for 20 min at 1190 °C. The 3 mm and 1 mm thick c-oriented plates were cut along the c-axis of the crystals and then polished to optical grade. The distance between the top and bottom part was about 4 cm.

The UV absorption edge wavelength and OH$^-$ spectra of 1-mm-thick plates were measured at room temperature on using a Beckman DU-8B spectrophotometer and Magna-560 Fourier transform IR spectrophotometer, respectively. High-resolution X-ray rocking curves of 3 mm plates were recorded by a Bruker HRXRD-5000 to examine the crystalline quality of LN: Mg3 and LN: Mg5 crystals. The refractive index of 1-mm-thick plates was also measured by METRICON 2010/M prism coupler at 632.8 nm to evaluate the optical homogeneity.

3. Results and Discussions

3.1. Crystal Growth

It is well known that heavily doped LN:Mg crystals remarkably increase the laser damage threshold [37]. However, with the increase in the concentration of MgO, the heavily Mg-doped LN crystals used in optical devices have always been inhomogeneous with low production efficiency using the Czochralski method. Besides, many defects, such as scattering particles and inclusions, have been found in heavily doped LN:Mg crystals. In order to grow Ø2″ optical grade heavily doped LN: Mg crystals with high homogeneity, more attention should be paid to its polycrystalline powders preparation, thermal field design, and growth technologies.

Normally, the LN:Mg polycrystalline powders are synthesized through solid reaction, which is mixing Li_2CO_3, Nb_2O_5, and MgO powders and then sintering at about 1100 °C [15]. Though the reaction of Nb_2O_5 with Li_2O, discomposed by Li_2CO_3, could produce LN easily, MgO has very high melt point (2800 °C), weak reaction activity, and low diffusion velocity, which cause difficulties in preparing homogeneous LN:Mg polycrystalline powders and might induce macroscopic inclusions in crystals. Higher reaction temperature or heat preservation with a long time might improve the uniformity of dopant in the polycrystalline powders or melt. However, it is easy to cause the component deviation as the volatilization of Li_2O. Thus, we chose the wet chemistry method with the advantage of low reaction temperature, which was helpful to avoid Li_2O volatilization and enhance the composition homogeneity of LN:Mg. We tested the polycrystalline powders by an X-ray diffractometer, and the results are shown in Figure 1. Based on the PDF#74–2238, the XRD spectrum showed that the diffraction peaks and relative intensity of LN, LN: Mg3, and LN: Mg5 polycrystalline materials were very similar to those of lithium niobate without any obvious peak shift or second phase. That indicated that LN could be successfully prepared by the wet chemical method, and doping Mg^{2+} had a negligible effect on diffraction data. Good quality of LN:Mg polycrystalline powders laid the foundation for crystal growth. Besides, most of doped LN crystals were grown by using pure LN crystals as seeds, but we used the Bridgman method to grow Ø1″ LN crystals with different concentrations of MgO and then cut as seeds for growing Ø2″ LN:Mg crystals.
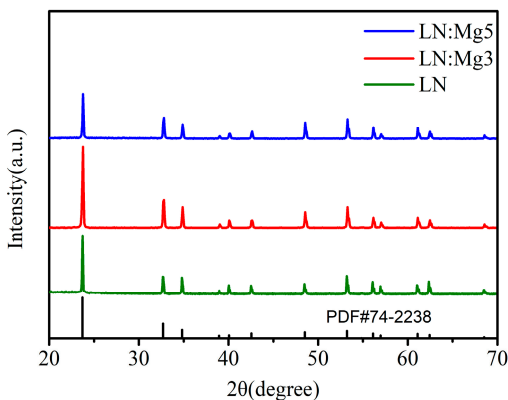
Figure 1. XRD results of LN:Mg polycrystalline powders prepared by the wet chemical method. LN—lithium niobate.

A stable and suitable thermal field is crucial to growing Ø2″ LN: Mg crystals with high quality. In the past, only Al_2O_3 powders were usually selected as insulation materials, but the heating time was long due to the low thermal conductivity of Al_2O_3 powders. In order to avoid the shortcomings, some mullite fiber was mixed with Al_2O_3 powders and served as insulation materials. About 35% of energy saving could be realized because of the higher thermal conductivity of mullite fiber compared to Al_2O_3 powders, which was also beneficial in keeping high stability of the thermal field. Moreover, with the excellent thermal insulation of mullite fiber mixed with Al_2O_3 powders, a small radial temperature gradient was obtained to avoid cracks caused by large thermal stress. The vertical temperature gradient $\left(\frac{\partial T}{\partial Z}\right)_s$ above the solid-melt interface was designed as 1 °C/mm, which was smaller than other LN crystals with a small diameter [27]. The reason is that the vertical temperature gradient, as seen from Equation (4), should be controlled in a certain range and has an inverse relationship with the diameter of the crystal [29].

$$\frac{2\varepsilon_b}{\alpha R^{3/2}} \bullet \left(\frac{2}{h}\right)^{1/2} \geq \left(\frac{\partial T}{\partial Z}\right)_s \geq \{-\frac{k_l m V_T(C_l(B)(1-k^*))}{D[k^* + (1-k^*)\exp(v_T\delta/D)]} + L\rho v_T\}/k_s \tag{4}$$

where α_a, ε_b, α,R, h,k_s, and v_T are the a-direction thermal expansion coefficient, fracture strain, thermal expansion coefficient, diameter, heat exchange coefficient, thermal conductivity, and falling rate (growth velocity of crystal), respectively; k_l and $C_l(B)$ are the thermal conductivity and bulk concentration of melt; m, δ,D, k^*, L, and ρ are the liquidus slope, depth of solute boundary layer, diffusion coefficient, segregation coefficient at the interface, crystalline latent heat and density, respectively. Besides, the falling rate was optimizing from 1.5 mm/h–2.0 mm/h to 0.5 mm/h–0.8 mm/h at different growth stages. In the crystal growth experiment, we set the descending speed to 0.5 mm/h and extended the holding time to 8 h, which was more conducive to Mg^{2+} entering the crystal lattice. The lower falling rate could provide enough time for the sufficient diffusion of Mg^{2+} at the solid-melt interface and improving Mg^{2+} distribution homogeneity in the crystal. The flat or slight convex shape was helpful to Mg^{2+} diffused along the vertical and parallel direction of the solid-melt interface.

Based on the above improvements, colorless, transparent, crack-free, and inclusions free LN:Mg single crystals were grown. The cut and polished LN: Mg5 crystal with a length of 4 cm is shown in Figure 2. High-resolution X-ray rocking curves are widely used in checking the crystalline quality of single crystals. The narrower full width at half maximum (FWHM) of single crystals means higher crystalline quality. Here, the X-ray rocking curves for c-plates of LN:Mg3 crystal and LN:Mg5 crystal are given in Figure 3. The FWHM was measured to be 8″ and 14″ for (001) reflection of LN:Mg5 and LN:Mg3 crystal, respectively, which was better than the reported results [38]. It implied that they possessed high structural quality with few dislocations and thermal stress [39]. This proved that the Bridgman method could grow LN:Mg crystals with higher crystallinity.
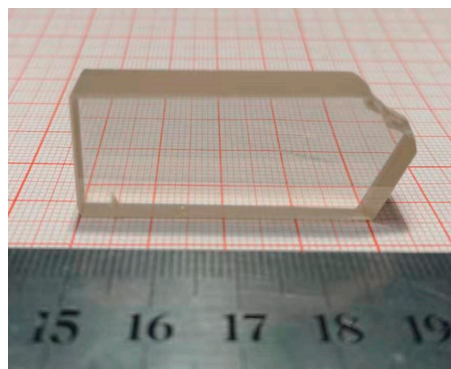
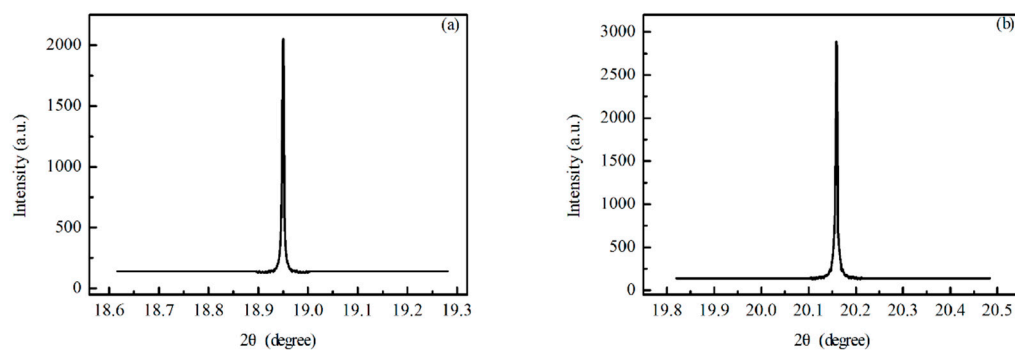**Figure 2.** Cut and polished LN: Mg5 crystal grew by the Bridgman method.

Figure 3. X-ray rocking curves of (001) reflection in LN:Mg crystals. (**a**) and (**b**) are for LN:Mg3 crystal and LN:Mg5 crystal, respectively.

3.2. Characterization

As we know, hydrogen ion can be introduced into LN crystals by means of water vapor during the growth of the crystals and forms as OH^- exists in the lattice. As OH^- is heavily sensitive to the surrounding environment, OH^- spectra are usually used to investigate the composition and defect structures of LN. An infrared absorption band near 2.87 μm (~3480 cm^{-1}) in pure LN crystal was first reported by Smith et al. [40]. Herrington et al. demonstrated that the absorption band was caused by the stretching vibrations of OH^- ions [41]. For doped LN crystals, it is well known that when the optical damage resistant dopants, such as Mg^{2+}, In^{3+}, and Hf^{4+}, are doped with the concentration exceeding their threshold, the OH^- absorption band shifts from the position at 3484 cm^{-1} of pure LN to higher wavenumbers [42,43]. As shown in Figure 4, LN and LN:Mg3 crystals showed a broad OH^- absorption band peak at approximately 3484 cm^{-1}, while the OH^- peak of LN:Mg5 crystal shifted to the higher wavenumber of 3534.7 cm^{-1}. It was proposed that in LN:Mg crystals, Mg^{2+} ions occupying Li-sites would push the Nb_{Li}^{4+} ions to the normal Nb-sites until all of the Nb_{Li}^{4+} were clean up when Mg concentration reached the threshold. Above the concentration threshold of Mg, additional Mg^{2+} ions would occupy Nb-sites. The position of 3534.7 cm^{-1} nearly coincided with the result of [42] and related to the OH^- vibration formation in (Mg_{Nb}^{2+}- OH^-) complex. It indicated that MgO was effectively doped into LN crystals, and 5 mol% had exceeded the threshold. Besides, as OH^- absorption band peaks of different positions in different plates or the same plate were nearly centered at the same wavenumber, it reflected that MgO distributed homogenously in LN:Mg5 crystal.
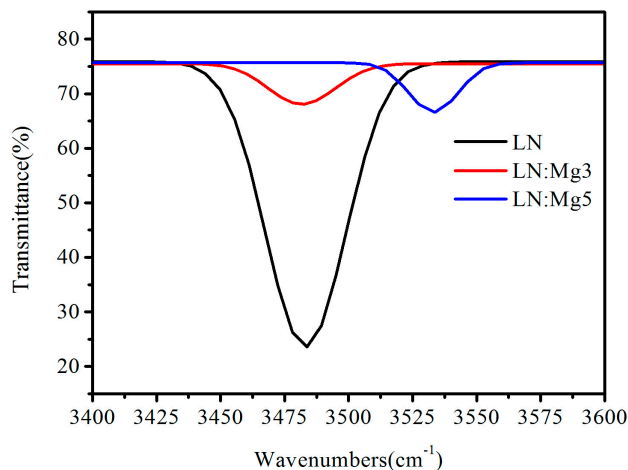
Figure 4. The OH⁻ spectroscopy of LN:Mg crystals.

Besides, the UV absorption edge of LN is also sensitive to defects [44]. Figure 5a shows that the UV absorption edge of LN:Mg3 and LN:Mg5 crystals was attributed to short wavelength compared to LN, especially the violet shift could be seen more obviously for LN:Mg5. The UV absorption edge of LN crystals has also been attributed to the presence of Li vacancies, actually of O^{2-} ions in the vicinity of V_{Li}^-, forming as the defect of $(V_{Li}^- - O^{2-})$ [45]. As mentioned above, for LN:Mg crystals, Mg^{2+} ions pushed the Nb_{Li}^{4+} ions to the normal Nb-sites and formed Mg_{Li}^{1+}, until all of the Nb_{Li}^{4+} dismissed when the MgO concentration exceeded the threshold. Compared with Nb_{Li}^{4+} that needs four cationic vacancies V_{Li}^- for keeping the electric charge equilibrium [46], Mg_{Li}^{1+} only needs one V_{Li}^- for charge compensation. Thereby, the decrement of the $(V_{Li}^- - O^{2-})$ defect concentration caused the observation of the UV absorption edge violet shift with the increment in MgO doping concentration. Especially, the Nb_{Li}^{4+} dismissal induced a more obvious violet shift in LN:Mg5 because of the MgO concentration exceeding the threshold. This result was also in accordance with the results of OH⁻ spectra. We also compared the transmittance of the top and bottom parts for LN:Mg5, as shown in Figure 5b. It was clear that the two curves almost coincided throughout the 4 cm long crystal, indicating the crystal possessed a nice uniformity.
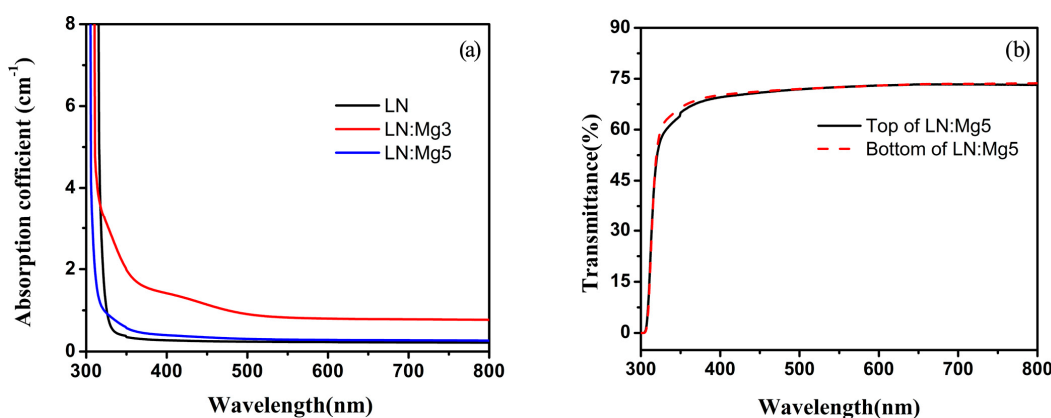

Figure 5. (**a**) is the UV absorption edge of LN:Mg crystals and (**b**) is the transmittance of the top and bottom plate in LN:Mg5 crystal.

High optical homogeneity is significant for the application of the nonlinear optical crystal. According to the high compositional homogeneity discussed above, LN:Mg5 crystal should also have high optical homogeneity. For the extraordinary refractive index n_e is sensitive to the composition while the ordinary refractive index n_o is not, the gradient of the extraordinary refractive index $\delta \triangle n_e$ was measured to examine the optical homogeneity of LN:Mg5 crystal. As listed in Table 1, the difference

between the average extraordinary refractive index $\delta\triangle n_e$ of the top and bottom plate in LN:Mg5 crystal was 1×10^{-4}. Since the distance of the two plates was about 4 cm, the gradient of the extraordinary refractive index $\delta\triangle n_e$ was about 2.5×10^{-5}/cm, which exhibited high optical homogeneity of the crystal. The optical homogeneity was about two times higher than the reported high optical homogeneous LN:Mg crystal, of which $\delta\triangle n_e$ was about 5.11×10^{-5}/cm [47].

Table 1. The extraordinary refractive index of the top and bottom plate in lithium niobate (LN):Mg5 crystal.

Samples	Extraordinary Refractive Index (n_e)					
	Position 1	Position 2	Position 3	Position 4	Position 5	Average
Bottom of LN:Mg5	2.1919	2.1917	2.1917	2.1918	2.1917	2.19176
Top of LN:Mg5	2.1916	2.1917	2.1918	2.1917	2.1915	2.19166

4. Conclusions

LN: Mg single crystals doped with different MgO concentrations were grown successfully in one furnace at the same time by the Bridgman method. Wet chemistry method was employed for LN: Mg polycrystalline powders preparation to enhance doping homogeneity of MgO and avoid Li_2O volatilization. The critical growth conditions included a small vertical temperature gradient, a low growth rate, adjusting the descending speed at different growth stages to keep a micro convex solid-melt interface. X-ray rocking curves of (001) reflection showed that the LN: Mg5 crystal had a high crystallinity. Compared with the congruent LN crystal, the OH^- absorption peaks and the ultraviolet absorption edge exhibited that the doping concentration of MgO exceeded the threshold. Moreover, LN: Mg5 crystal had high optical homogeneity for the extraordinary refractive index gradient that was as small as 2.5×10^{-5}/cm.

Author Contributions: T.T. conceived and designed the experiments. T.T., X.Y. and M.W. performed the experiments, analyzed the data. H.S., D.Z., and Y.Z. contributed the measurements. J.X. contributed useful and deep discussions. T.T. and X.Y. wrote the manuscript. All authors read and approved the final version of the manuscript to be submitted.

Conflicts of Interest: The authors declare no conflict of interest.

References

1. Wang, C.; Zhang, M.; Stern, B.; Lipson, M.; Loncar, M. Nanophotonic lithium niobate electro-optic modulators. *Opt. Express* **2018**, *26*, 1547–1555. [CrossRef] [PubMed]
2. Dhar, L.; Curtis, K.; Fäcke, T. Holographic data storage: Coming of age. *Nat. Photonics* **2008**, *2*, 403–405. [CrossRef]
3. Wang, Y.; Zhou, S.X.; He, D.H.; Hu, Y.; Chen, H.X.; Liang, W.G.; Yu, J.H.; Guan, H.Y.; Luo, Y.H.; Zhang, J.; et al. Electro-optic beam deflection based on a lithium niobate waveguide with microstructured serrated electrodes. *Opt. Lett.* **2016**, *41*, 4739–4742. [CrossRef] [PubMed]
4. Bazzan, M.; Sada, C. Optical waveguides in lithium niobate: Recent developments and applications. *Appl. Phys. Rev.* **2015**, *2*, 040603. [CrossRef]
5. Jiang, H.W.; Luo, R.; Liang, H.X.; Chen, X.F.; Chen, Y.P.; Lin, Q. Fast response of photorefraction in lithium niobate microresonators. *Opt. Lett.* **2017**, *42*, 3267–3270. [CrossRef]
6. Tu, D.; Xu, C.N.; Yoshida, A.; Fujihala, M.; Hirotsu, J.; Zheng, X.G. $LiNbO_3$:Pr^{3+}: A multipiezo material with simultaneous piezoelectricity and sensitive piezoluminescence. *Adv. Mater.* **2017**, *29*, 1606914. [CrossRef]
7. Gopalan, K.K.; Janner, D.; Nanot, S.; Parret, R.; Lundeberg, M.B.; Koppens, F.H.L.; Pruneri, V. Mid-infrared pyroresistive graphene detector on $LiNbO_3$. *Adv. Opt. Mater.* **2017**, *5*, 1600723. [CrossRef]

8.　Ballman, A.A. Growth of piezoelectric and ferroelectric materials by the CzochraIski technique. *J. Am. Ceram. Sot.* **1965**, *48*, 112–113. [CrossRef]

9.　Lengyel, K.; Péter, Á.; Kovács, L.; Corradi, G.; Pálfalvi, L.; Hebling, J.; Unferdorben, M.; Dravecz, G.; Hajdara, I.; Szaller, Z. Growth, defect structure, and THz application of stoichiometric lithium niobate. *Appl. Phys. Rev.* **2015**, *2*, 040601. [CrossRef]

10.　Hesselink, L.; Orlov, S.S.; Liu, A.; Akella, A.; Lande, D.; Neurgaonkar, R.R. Photorefractive materials for nonvolatile volume holographic data storage. *Science* **1998**, *282*, 1089–1094. [CrossRef]

11.　Schmidt, W.G.; Albrecht, M.; Wippermann, S.; Blankenburg, S.; Rauls, E.; Fuchs, F.; Rödl, C.; Furthmüller, J.; Hermann, A. LiNbO$_3$ ground- and excited-state properties from first-principles calculations. *Phys. Rev. B* **2008**, *77*, 035106. [CrossRef]

12.　Bernert, C.; Hoppe, R.; Wittwer, F.; Woike, T.; Schroer, C.G. Ptychographic analysis of the photorefractive effect in LiNbO$_3$:Fe. *Opt. Express* **2017**, *25*, 31640–31650. [CrossRef] [PubMed]

13.　Yang, Y.P.; Buse, K.; Psaltis, D. Photorefractive recording in LiNbO$_3$:Mn. *Opt. Lett.* **2002**, *27*, 158–160. [CrossRef] [PubMed]

14.　Ren, L.Y.; Liu, L.R.; Liu, D.A.; Zu, J.F.; Luan, Z. Optimal switching from recording to fixing for high diffraction from a LiNbO$_3$:Ce:Cu photorefractive nonvolatile hologram. *Opt. Lett.* **2004**, *29*, 186–188. [CrossRef]

15.　Wang, S.; Ji, C.; Dai, P.; Shen, L.; Bao, N. The growth and characterization of six inch lithium niobate crystal with high homogeneity. *Cryst. Eng. Comm.* **2020**. [CrossRef]

16.　Byer, R.L.; Young, J.F.; Feigelson, R.S. Growth of high-quality LiNbO$_3$ crystals from the congruent melt. *J. Appl. Phys.* **1970**, *41*, 2320–2325. [CrossRef]

17.　O'BRYAN, H.M.; Gallagher, P.K.; Brandle, C.D. Congruent composition and Li-rich phase boundary of LiNbO$_3$. *J. Am. Ceram. Soc.* **1985**, *68*, 493–496. [CrossRef]

18.　Ashkin, A.; Boyd, G.D.; Dziedzic, J.M.; Smith, R.G.; Ballman, A.A.; Levinstein, J.J.; Nassau, K. Optically-induced refractive index inhomogeneities in LiNbO$_3$ and LiTaO$_3$. *Appl. Phys. Lett.* **1966**, *9*, 72–74. [CrossRef]

19.　Zhong, G.G.; Jian, J.; Wu, Z. Measurement of optically induced refractive-index damage of lithium niobate doped with different concentrations of MgO. *J. Opt. Soc. Am.* **1980**, *70*, 631.

20.　Liu, J.J.; Zhang, W.L.; Zhang, G.Y. Defect chemistry analysis of the defect structure in Mg-doped LiNbO$_3$ crystals. *Phys. Stat. Sol(A).* **1996**, *156*, 285–291. [CrossRef]

21.　Yao, L.F.; Li, J.L.; Liu, J.H.J. The study of growth on magnesium doped lithium niobate crystals. *J. Changchun Inst. Opt. Fine Mech.* **1994**, *17*, 65–68.

22.　Kim, I.W.; Park, B.C.; Jin, B.M.; Bhalla, A.S.; Kim, J.W. Characteristics of MgO-doped LiNbO$_3$ crystals. *Mater. Lett.* **1995**, *24*, 157–160. [CrossRef]

23.　Bae, S.I.; Ichikawa, J.; Shimamura, K.; Onodera, H.; Fukuda, T. Doping effects of Mg and/or Fe ions on congruent LiNbO$_3$ single crystal growth. *J. Cryst. Growth.* **1997**, *180*, 94–100. [CrossRef]

24.　Chen, Y.L.; Guo, J.; Lou, C.B.; Yuan, J.W.; Zhang, W.L.; Chen, S.L.; Zhang, G.Y. Crystal growth and characteristics of 6.5 mol% MgO-doped LiNbO$_3$. *J. Cryst. Growth.* **2004**, *263*, 427–430. [CrossRef]

25.　Palatnikov, M.N.; Birukova, I.V.; Masloboeva, S.M.; Makarova, O.V.; Manukovskaya, D.V.; Sidorov, N.V. The search of homogeneity of LiNbO$_3$ crystals grown of charge with different genesis. *J. Cryst. Growth.* **2014**, *386*, 113–118. [CrossRef]

26.　Yoshimura, M.; Sakata, S.I.; Iba, H.; Kawano, T.; Hoshikawa, K. Vertical Bridgman growth of Al$_2$O$_3$/YAG: Ce melt growth composite. *J. Cryst. Growth.* **2015**, *416*, 100–105. [CrossRef]

27.　Shi-Ji, F.; Guan-Shun, S.; Wen, W.; Jin-Long, L.; Xiu-hang, L. Bridgman growth of Li$_2$B$_4$O$_7$ crystals. *J. Cryst. Growth.* **1990**, *99*, 811–814. [CrossRef]

28.　Nishimura, E.; Okano, K.; Iida, J.; Hoshikawa, K. LiTaO$_3$ Single Crystal Growth by the Vertical Bridgman Technique. *Crystl. Res. Technol.* **2018**, *53*, 1800044. [CrossRef]

29.　Liu, W.B.; Tian, T.; Yang, B.B.; Xu, J.Y.; Liu, H.D. Bridgman growth and luminescence properties of dysprosium doped lead potassium niobate crystal. *J. Cryst. Growth.* **2017**, *468*, 462–464. [CrossRef]

30.　Jin, M.; Lin, S.; Li, W.; Chen, Z.; Li, R.; Wang, X.; Pei, Y. Fabrication and thermoelectric properties of single-crystal argyrodite Ag8SnSe6. *Chem. Mater.* **2019**, *31*, 2603–2610. [CrossRef]

31.　Jin, M.; Shen, H.; Fan, S.J.; He, Q.B.; Xu, J.Y. Industrial growth and characterization of Si-doped GaAs crystal by a novel multi-crucible Bridgman method. *Cryst. Res. Technol.* **2017**, *52*, 1700052. [CrossRef]

32. Chen, H.; Xia, H.; Wang, J.; Zhang, J.; Xu, J.; Fan, S. Growth of LiNbO$_3$ crystals by the Bridgman method. *J. Cryst. Growth.* **2003**, *256*, 219–222. [CrossRef]

33. Xu, X.; Liang, X.; Li, M.; Solanki, S.; Chong, T.C. Two-color nonvolatile holographic recording in Bridgman-grown Ru: LiNbO$_3$ crystals. *J. Cryst. Growth.* **2008**, *310*, 1976–1980. [CrossRef]

34. Iyi, N.; Kitamura, K.; Yajima, Y.; Kimura, S.; Furukawa, Y.; Sato, M. Defect structure model of MgO-doped LiNbO$_3$. *J. Solid. State. Chem.* **1995**, *118*, 148–152. [CrossRef]

35. Niwa, K.; Furukawa, Y.; Takekawa, S.; Kitamura, K. Growth and characterization of MgO doped near stoichiometric LiNbO$_3$ crystals as a new nonlinear optical material. *J. Cryst. Growth.* **2000**, *208*, 493–500. [CrossRef]

36. Furukawa, Y.; Sato, M.; Nitanda, F.; Ito, K. Growth and characterization of MgO-doped LiNbO$_3$ for electro-optic devices. *J. Cryst. Growth.* **1990**, *99*, 832–836. [CrossRef]

37. Bryan, D.A.; Gerson, R.; Tomaschke, H.E. Increased optical damage resistance in lithium niobate. *Appl. Phy. Lett.* **1984**, *44*, 847–849. [CrossRef]

38. Bhatt, R.; Bhaumik, I.; Ganesamoorthy, S.; Bright, R.; Soharab, M.; Karnal, A.K.; Gupta, P.K. Control of intrinsic defects in lithium niobate single crystal for optoelectronic applications. *Crystals.* **2017**, *7*, 23. [CrossRef]

39. Yao, S.H.; Hu, X.B.; Wang, J.Y.; Liu, H.; Chen, X.F. Growth and characterization of near stoichiometric LiNbO$_3$ single crystal. *Cryst. Res. Technol.* **2007**, *42*, 114–118. [CrossRef]

40. Smith, R.G.; Fraser, D.B.; Denton, R.T.; Rich, T.C. Correlation of reduction in optically induced refractive index inhomogeneity with OH content in LiTaO$_3$ and LiNbO$_3$. *J. Appl. Phys.* **1968**, *39*, 4600–4602. [CrossRef]

41. Herrington, J.R.; Dischler, B.; Räuber, A.; Schneider, J. An optical study of the stretching absorption band near 3 microns from OH$^-$ defects in LiNbO$_3$. *Solid State Commun.* **1973**, *12*, 351–354. [CrossRef]

42. Kong, Y.F.; Deng, J.C.; Zhang, W.L.; Wen, J.K.; Zhang, G.Y.; Wang, H.F. OH$^-$ absorption spectra in doped lithium niobate crystals. *Phys. Lett. A* **1994**, *196*, 128–132. [CrossRef]

43. Kokanyan, E.P.; Razzari, L.; Cristiani, I.; Degiorgio, V.; Gruber, J.B. Reduced photorefraction in hafnium-doped single-domain and periodically poled lithium niobate crystals. *Appl. Phys. Lett.* **2004**, *4*, 1880–1882. [CrossRef]

44. Földvári, I.; Polgár, K.; Voszka, R.; Balasanyan, R.N. A simple method to determine the real composition of LiNbO$_3$ crystals. *Cryst. Res. Technol.* **1984**, *19*, 1659–1661. [CrossRef]

45. Li, X.; Kong, Y.; Liu, H.; Sun, L.; Xu, J.; Chen, S.; Zhang, G. Origin of the generally defined absorption edge of non-stoichiometric lithium niobate crystals. *Solid State Commun.* **2007**, *141*, 113–116. [CrossRef]

46. Kityk, I.V.; Makowska-Janusik, M.; Fontana, M.D.; Aillerie, M.; Abdi, F. Nonstoichiometric defects and optical properties in LiNbO$_3$. *J. Phys. Chem. B.* **2001**, *105*, 12242–12248. [CrossRef]

47. Ferriol, M.; Dakki, A.; Cohen-Adad, M.T.; Foulon, G.; Boulon, G. Growth and characterization of mgo-doped single-crystal fibers of lithium niobate in relation to high temperature phase equilibria in the ternary system Li$_2$O-Nb$_2$O$_5$-MgO. *J. Cryst. Growth.* **1997**, *178*, 529–538. [CrossRef]